Microstructural Analysis of Friction Stir Weld Joints between Ni-Based Alloy 625 and Mild-Carbon Steel A516

Undergraduate Thesis

Presented in Partial Fulfillment of the Requirements for Graduation with Honors Research Distinction in the College of Engineering of The Ohio State University

Genevieve Wai-Yin Lee

Welding Engineering Program

The Ohio State University

2016

Defense Committee:

Dr. Antonio J. Ramirez, Ph.D., Advisor

Dr. David Phillips, Ph.D.

Abstract

Welds between Ni-based alloys and steels are often sought after for the combination of inexpensive material with moderate to high strength in combination and superior corrosion resistance, namely within industries requiring high-performance materials functioning in harsh, corrosive environment exposure. Fusion welds between the two alloys are currently used in industry, and Solid-State welds between these alloys may be a potential candidate to join these materials. Friction Stir Welds (FSW) between Ni-based alloy 625 and Low-Carbon Steel ASTM A516 have been studied previously, but not extensively under micron-scale resolutions. Advanced electron microscopy characterization is used to analyze these joints at resolutions up to approximately 10 nm.

This study follows the development and application of Transmission Kikuchi Diffraction (TKD), a microscopy method akin to Electron BackScatter Diffraction (EBSD) in the Scanning Electron Microscope (SEM) on samples at the interface of FSW between Ni-based Alloy 625 and Steel A516. Analyses are run in combination with Energy Dispersive X-ray Spectroscopy (X-EDS), and microstructural, crystallographic, and chemical data are reported within this study. Crystallographic interface of iron Ferrite and nickel Austenite is observed with TKD at the weld interface. Fine, possibly strained, 300 nm grains adjacent to this interface are indicative of martensite or residual strains from the FSW process, and precipitates in the Austenitic matrix can be seen within grains and grain boundaries. A gradient elemental interdiffusion region of iron, nickel, chromium is detected by X-EDS within the FCC Austenite region, and precipitates appear to contain niobium and molybdenum.

Acknowledgements

I wish to express my sincere gratitude to my research advisor, Antonio J Ramirez, for his help and guidance on this project. His support has been a driving factor in the direction and the quality of the work done and knowledge gained throughout my journey conducting research. I would also like to express my deepest appreciation to Jonathan Orsborn at CEMAS who worked to teach me SEM analysis and helped with all things TKD related. Without him, any work and development in electron microscopy would not have been completed so swiftly and adeptly. Finally, many thanks to Sebastian Romo-Arango for his guidance and support on this project.

Table of Contents

List of Tables

List of Figures

Chapter 1: Introduction and Motivation

Fuel and energy is consumed endlessly and its usage is common worldwide, making the oil-and gas industry a profitable sector and a considerable part of the economy. These industries store and transport caustic and often dangerous fluids to and from highly corrosive or harsh marine environments. The integrity of these structures must be kept at high standards and require the use of high-performance materials to meet all necessary criteria, as failures can be catastrophic with far-reaching consequences, both economically and ecologically.

Often, Nickel-based alloys are used for their excellent resistance to corrosive and marine environment exposure and strength. Their high costs drive designers and engineers to find more cost-efficient alternatives to using solely Ni-based alloys in oil and gas structures. One standard alternative is to fusion weld Ni-based alloy with steel to offset the high cost, but there are often weldability issues associated with it. These alloys exhibit distinct material and physical properties, particularly at high temperatures, and when they melt and solidify during the fusion weld process, defects such as solidification cracking, embrittlement, and voids can present.

Solid-state (SS) welding is a method that metallurgically bonds metals together without exceeding melting temperatures. These welds between nickel-based alloys and steels are not commonly implemented in industrial applications, and studies in this topic are not extensive. Research on and characterization of Friction Stir Welds (FSW)

between Ni-based alloy 625 and Low-Carbon Steel ASTM A516 has been conducted, but not extensively at spatial resolution below the micron-level. Further investigation of these joints is necessary to provide adequate data in pushing this process toward manufacturing applications.

Transmission Kikuchi Diffraction (TKD) is an advanced electron microscopy method that can be conducted using the Scanning Electron Microscope (SEM) to produce crystallographic information on thin foils. In conjunction with Energy Dispersive X-ray Spectroscopy (X-EDS) which identifies chemical composition, thorough characterization of samples can be completed up to 10 nm resolutions. In this study, the development of TKD on Electron BackScatter Diffraction (EBSD) software and equipment is detailed as well as its application on FSW between Ni-based alloy and low-carbon steels. In developing TKD, other research groups will have access to it and further data collection and knowledge gained in their respective subjects where such high resolutions were not feasibly attained previously.

Chapter 2: Background

2.1 Dissimilar Metal Welds

Dissimilar metal welds are commonly used in welding, and there are many inherent issues that result from such practices. Mechanically, the joint between two dissimilar metals will suffer due to the mismatch of base material physical properties, enhanced by the elevated thermal cycles of weld processes. Disparities between thermal expansions, melting points, thermal conductivities, and many more physical properties can cause a multitude of mechanical problems ranging from intense residual stresses, uneven melting and mixing of base materials, and voids or porosity from the different degrees of thermal contraction. Typically, material selection and post-weld processing considerations combat these issues.

Metallurgically, dissimilar metal welds contain a gradient intermixing region, especially within fusion welded samples, where diffusion among base metals can create a host of material issues that result in susceptibility in physical and metallurgical integrity. Specifically in Ni-based alloy and steel, there are often instances of dilution of the nickel alloy by the steel, causing martensitic transformation, commonly seen in many fusion welds [1]. This can be detrimental to joints, as the brittle phase can cause catastrophic failure far below expected performances. The greater nickel content will increase the stability of austenite in steels upon cooling, and expand the opportunity for transformation to martensite, even in low-carbon steel alloys. This embrittling

phenomena has been documented in many studies and even within industry when joining steels and nickel alloys [2].

2.2 Solid-State Welding

Often, welds will be made in the solid state in order to circumvent weldability issues caused by fusion welds, such as solidification cracking, porosity, and embrittlement in the weld zone – especially in dissimilar metal welds. SS weld processes utilize forging and plasticizing of solid metal to induce material flow and form a bonded joint. Thus, low-temperature melting, soft materials such as aluminum and magnesium are more commonly joined in this manner.

Sound metallurgical bonds between metals can be made without melting when nascent material of base metals are brought into close proximity on the order of nanometers [3]. Usually, oxides, surface contamination, and asperities prevent SS, or cold welding, and a combination of heat, temperature, or time is used in weld processes to produce a SS bond. SS weld methods such as Friction Stir Welding, Explosion or Impact welding, Ultrasonic welding, or Roll-bonding are among many processes that are used to create such joints.

Studies in SS welding of nickel alloys, show stir zone microstructure to contain a Face-Centered Cubic (FCC) Austenitic nickel matrix and various precipitates. Segregation and re-precipitation occurs in fast, low thermal cycle SS welds like linear friction welding [4] [5], while distribution of precipitates is more commonly observed in slower SS joining methods like Friction Stir Welding (FSW) [6] [7]. In both studies, intense recrystallization occurred throughout the weld process due to the low stacking fault energy of the FCC crystal lattice. Peak temperatures of FSW within these alloys

reach approximately 800°C, and in solid-solution strengthened nickel alloys, MC carbides such as niobium and titanium carbides are dispersed within the stir zone. Ni_3Nb (γ") and M_6C carbides are observed in the stir zone when post-processing is applied after FSW about 20-80 nm large.

In steels, SS welding can provide many advantages with respect to metallurgical structure and thermal processing. Some steels can undergo phase transformations to brittle martensite if cooled too fast from the Austenitization temperature, usually around 700-800°C, denoted in Figure 1. Carbon in steels increases the formation of γ-austenite phase at elevated temperatures and swift cooling prevents diffusion of the alloying element throughout the material, causing diffusionless, "displacive" or "military" transformation of the crystal lattice to the brittle martensite often seen in stir zones of higher carbon steels.

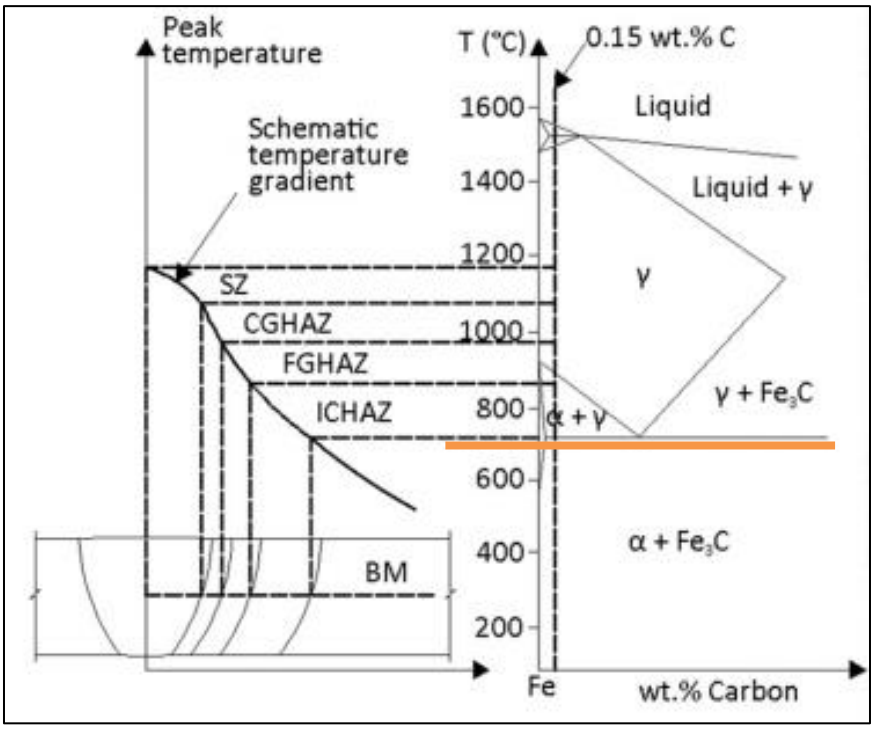

Figure 1. Steel Phases and Weld Peak Temperatures

Since SS weld methods produce much lower peak temperatures, martensite in these materials may be prevented, and post-weld heat treatments of such joints can be bypassed. Current literature on SS welds of carbon steels show improved mechanical properties at weld areas when compared to base metal in both mild carbon steels and high-carbon steels [8] [9].

In dissimilar bonds, welds in the solid state will decrease the opportunity for mixing and diffusion comparatively due to the lack of melting and liquid diffusion between the two base materials. Dissimilar SS bonds between Ni-based alloys and steels should exhibit much less embrittlement compared to their fusion welded counterparts, because of the reduced susceptibility to martensitic phase transformation [10].

2.3 Friction Stir Welding

Friction Stir Welding is a solid-state welding method developed by TWI in 1991 [11] that has made its way into manufacturing processes today. Formerly only used heavily in the aerospace industry, it is now being introduced to automotive production to join dissimilar welds between nickel alloys and steels. FSW can produce high quality joints that do not require any post processing, but are dramatically slower when compared to other weld processes. This method of creating metallic joints can often result in greater thermomechanical properties since temperatures are kept below melting: adverse thermal cycles that detrimentally affect microstructures are avoided, and stirring mechanism often refines the grain sizes, improving yield and tensile strengths [5] [6].

FSW is used to create a metallurgical bond between two materials, usually in a butt or lap joint configuration, exemplified in Figure 2.

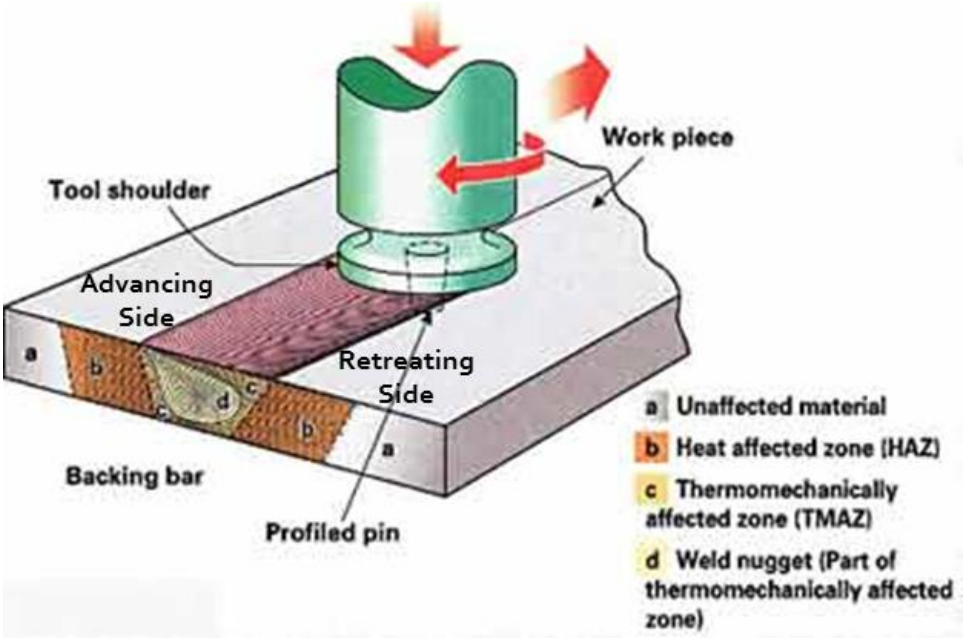

Figure 2. Friction Stir Weld Parts [12]

In this process, a threaded pin and shoulder tooling, rotates and plunges into the solid joint interface, generating frictional and deformational heating. Base plates are clamped down tightly to ensure quality joint fit up in the presence of the intense stresses that are produced in the process. As heat continues to be generated, the rotating pin traverses along the length of the weld, plasticizing, extruding, and forging the material around it.

The cross section of the weld is similar to that of a fusion weld, where a weld nugget and thermo-mechanically affected zone is akin to the fusion zone, and a heat affected zone exists in both. The thermo-mechanically affected zone is the area where material flow has been induced to form the metallurgical bond between base metals. Because the tool is rotating in one direction, the resulting weld nugget, or "stir zone," of the thermo-mechanically affected is asymmetric, described by an Advancing and Retreating side. The advancing side undergoes more shearing and mixing as the pin rotates in the direction opposing weld travel direction. The retreating side rotates in the

same direction as weld travel, and consequently sees a lesser degree of grain refinement and material mixing.

Although this process may circumvent many physical and material weldability issues related to fusion weld methods, there is a unique set of defects that may present when making FSW. Wormholes, or voids in in the thermo-mechanically affected zone, lack of penetration, lack of fusion may be formed where there exists some incomplete bonding or consolidation of the base materials. Additionally, with incorrect process parameters there may also be finishing or aesthetic defects such as excess flash, indentation or root flow. These are common defects that may be avoided with careful optimization of weld parameters such as tool RPM, weld travel speed, pin tool offset, and axial, or downward, force of the pin and shoulder tool. Many individuals have conducted optimization of FSW on various materials and joint configurations in order to produce welds that are mechanically and metallurgically sound which require no post-weld processing.

J. Rodriguez and A. J. Ramirez have completed a study on the optimization of FSW between Ni-based alloy 625 and ASTM A516 Steel [13]. Optimal welds were made using a W-Re/PCBN (Tungsten-Rhenium Polycrystalline Cubic Boron Nitride) composite tool. The tool had a shoulder diameter of 26.0 mm and pin length of 6.1 mm and diameters of 3.9 and 10.0 mm at the smallest and largest widths of pin threading. They found the optimal weld speed of 100 mm/min, rotational speed of 300 rev/min, a tool offset of 1.63 mm at 30 kN of downward force.

2.4 Transmission Kikuchi Diffraction

Transmission Kikuchi Diffraction is an electron microscopy technique that analyzes crystallographic information, nearly identical to EBSD. The main difference between the two methods is that TKD utilizes thin foil samples to obtain diffraction patterns via electron transmission, where EBSD collects diffraction patterns formed by electron backscattering, below in Figure 3 and Figure 4. This modification allows TKD to resolve data points at much higher resolution due to significantly reduced electron scattering.

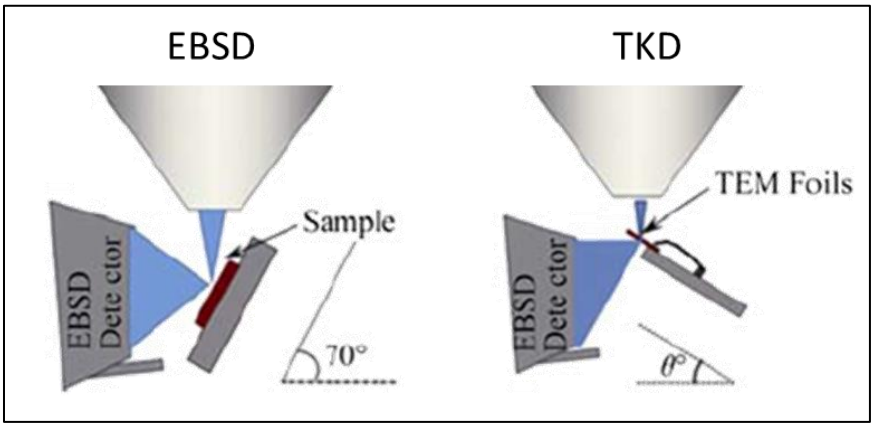

Figure 3. TKD and EBSD Configuration [14]

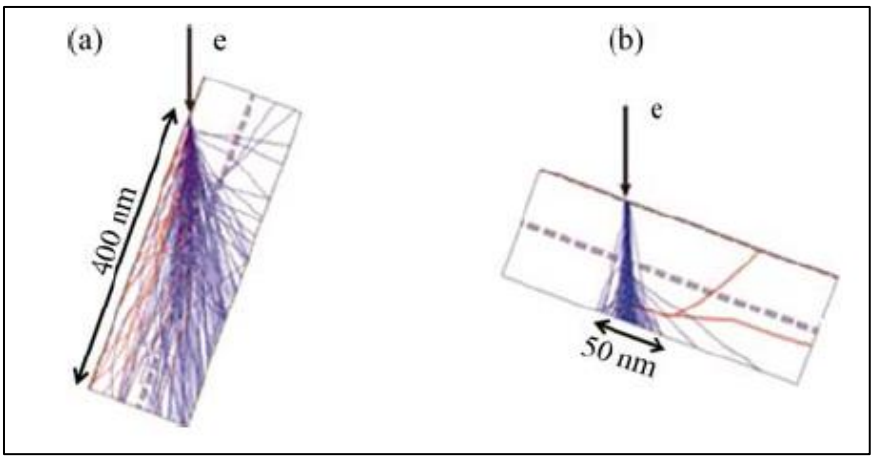

Figure 4. TKD and EBSD Electron Scattering [14]

EBSD and TKD obtain crystallographic information by the production of Transmission Kikuchi Patterns (TKP) diffraction patterns by the diffraction and detection of coherent electrons. These TKP diffraction patterns are produced when the Bragg condition is satisfied by the crystal planes in the tilted sample, and coherent electrons are diffracted in specific orientations at that Bragg angle. Thus, wide opposing ‘cones’ of coherent electron signal originating from the interaction volume of the sample, called Kossel cones, create the near-linear patterns observed in a TKP, demonstrated in Figure 5 [15]. In this manner, TKD provides crystal structure information, which can discern lattice spacing of certain groups, crystal systems, and orientation of individual crystals among other things.

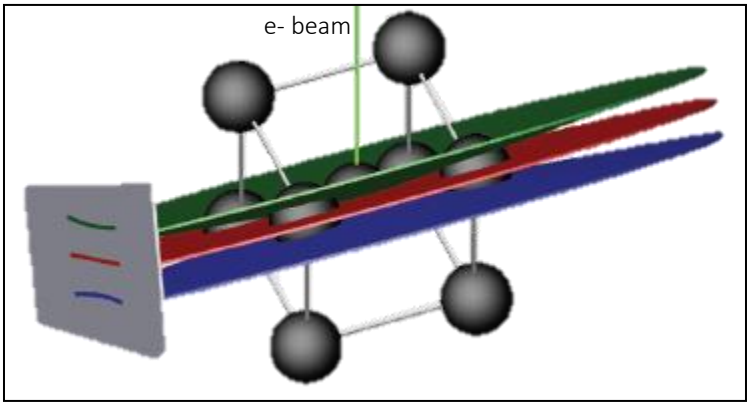

Figure 5. Production of TKPs by Diffraction Plane [16]

Diffraction patterns originate from the bottom 20 nm of the sample foil. This allows transmission of patterns from foil thicknesses ranging from 5 nm to upwards of 3 microns thick [17], but general success has been seen in the range of 200-500 nm of foil thickness. Additionally, studies have shown that the highest resolution step size that produces an evident effect on mapping is of 10 nm [18]. Software has been developed to distinguish these bands and extract information from them, and automation of such processes have brought about rapid characterization of specimens.

Ideally, analysis of samples can yield accurate crystallographic data of all distinct phases. Often, TKD alone will not conclusively identify phases within a sample, as there is error associated with this process as with all other analyses. Signal noise and charging may contribute to the quality of TKPs, in addition to strain and dislocations contained within a crystal lattice. Furthermore, parameters of each phase must be known and supplied to the software for phase identification. Lattice spacing parameters, crystal symmetry, and the crystal unit cell structure are parts of a complete phase profile that EBSD software uses to assign phase identification. Even then, there may be error in these values that can cause incorrect identification of phases, especially when TKPs of different phases can produce similar looking patterns.

To obtain successful characterization analyses of samples, X-EDS is regularly used in combination with TKD to provide conclusive data on sample make-up. X-EDS is used to complement the crystallographic data by provision of chemical composition data. Distinct elements can be identified by the characteristic X-rays that are produced when elements interact and absorb electrons from the electron beam. Each element produces x-rays of distinct energy values, and when paired with TKD, more accurate characterization of samples can be achieved.

Chapter 3: Experimental Parameters and Testing Setup

3.1 Material and Weld Parameters

Friction Stir Welds were made between 6.6 mm thick plates of Ni-Based Alloy 625 and Mild Carbon Steel ASTM A516 in a butt joint configuration. Chemical compositions of plate alloys can be seen in Table 1 below [17].

Table 1
Chemical Compositions (wt%) of ASTM A516 Gr 60 Steel and Ni-based Alloy 625

Element	Ni	Cr	Mo	Nb	Fe	Si	Ti	Al	Mn	Co	C
A516*	0.01	0.03	–	–	Bal	0.25	–	0.29	0.95	–	0.15
A625*	60.72	22.59	9.39	3.50	3.,00	0.22	0.24	0.18	0.09	0.05	0.02

* Chemical composition provided by the manufacturer.

The FSW was created with a W-Re/PCBN (Tungsten-Rhenium Polycrystalline Cubic Boron Nitride) composite tool with a shoulder diameter at 26.0 mm and pin dimensions 6.1 mm length by threaded diameters of 3.9 and 10.0 mm at the smallest and largest widths. The weld was made at a weld speed of 100 mm/min, rotational speed of 300 rev/min, a tool axial offset O_A of 1.63 mm toward the steel plate, and 30 kN axial force as seen in Figure 6 below [17].

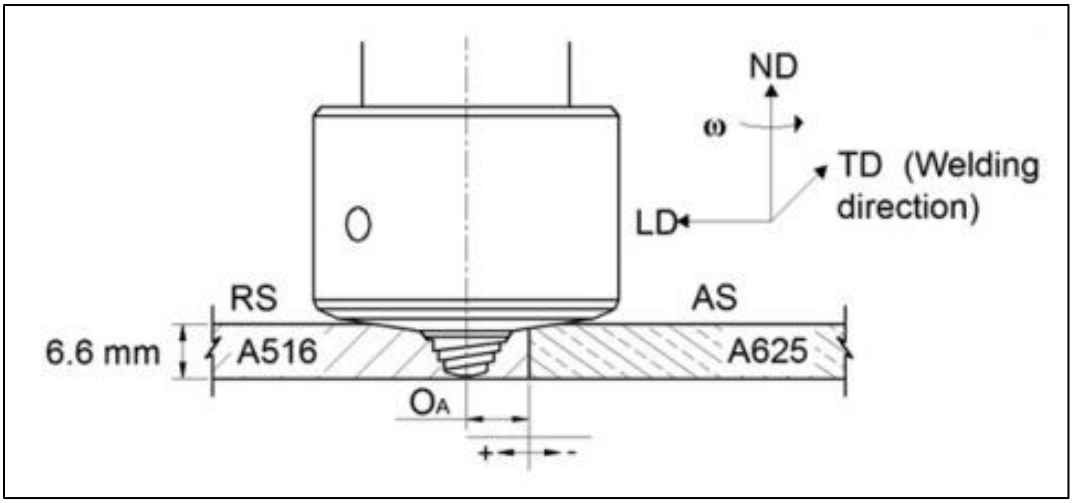

Figure 6. Diagram of FSW Configuration

3.1 TKD Sample Holder

Because TKD had not been successfully conducted at the Center for Electron Microscopy (CEMAS) prior to this project, modifications to the EBSD process were necessary in order to proceed with analyses on the samples. A suitable sample holder for the thin foils used in simultaneous TKD is required to be stable with ease of insertion and removal of the thin foil. In order to use the holder for simultaneous TKD and X-EDS analysis, it must not contain any elements of interest present in the sample; have a thin cross section, particularly at areas adjacent to the thin foil; and virtually no material volume underneath the electron beam to reduce noise from the holder material. In Figure 7 below, the TKD sample holder designed by Oxford Instrumentation is shown [18], exhibiting the aforementioned characteristics. Following images in Figure 8 - Figure 10 present prototype designs of various alloys.

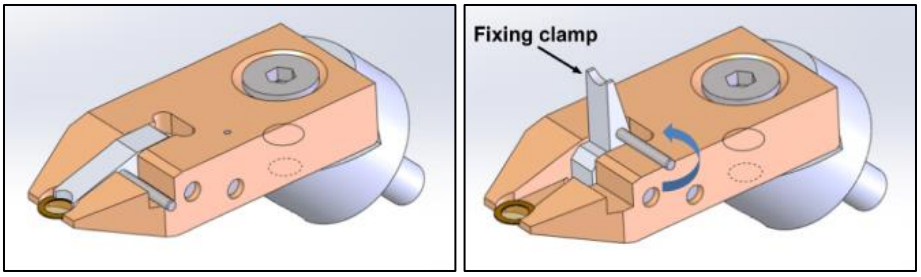

Figure 7. Oxford Instrumentation TKD Holder

Figure 8 depicts the aluminum TKD holder designed and built by Sebastián Romo Arango, and Figure 9 is another TKD holder that utilizes steel razor blades and an aluminum SEM finger that is designed and assembled by Jonathan Orsborn for used for preliminary TKD testing only. The aluminum holder has a 5 mm wide body and a 60° pre-tilt, and the steel holder has a 45° tilt. The Figure 10 is a second iteration of the aluminum design created in graphite also by S.R. Arango. The graphite holder exhibits the same general features of the aluminum holder, but possesses a thinner clamping area near the thin foil, and a wider body, and a 45° pre-tilt. Silver paint was used to attach both aluminum and graphite holders to the aluminum SEM stub for conductivity. The aluminum holder in the figure does not show the SEM stub or screw and springs assembled like the graphite holder in Figure 10.

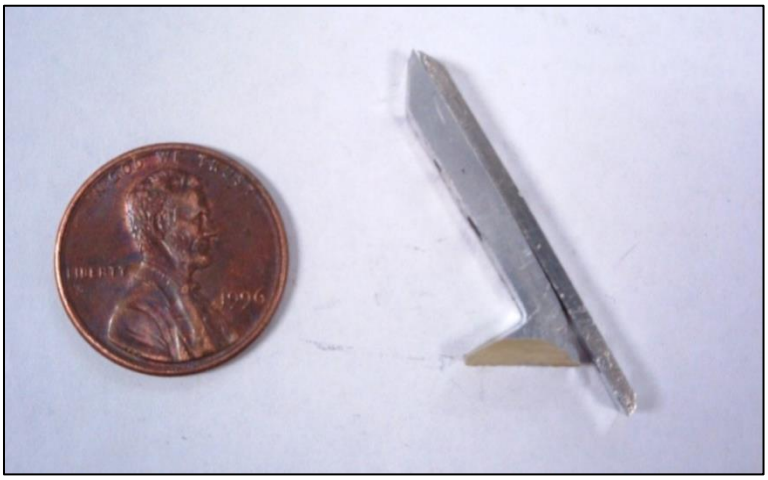

Figure 8. Aluminum TKD Holder Prototype by S. R. Arango

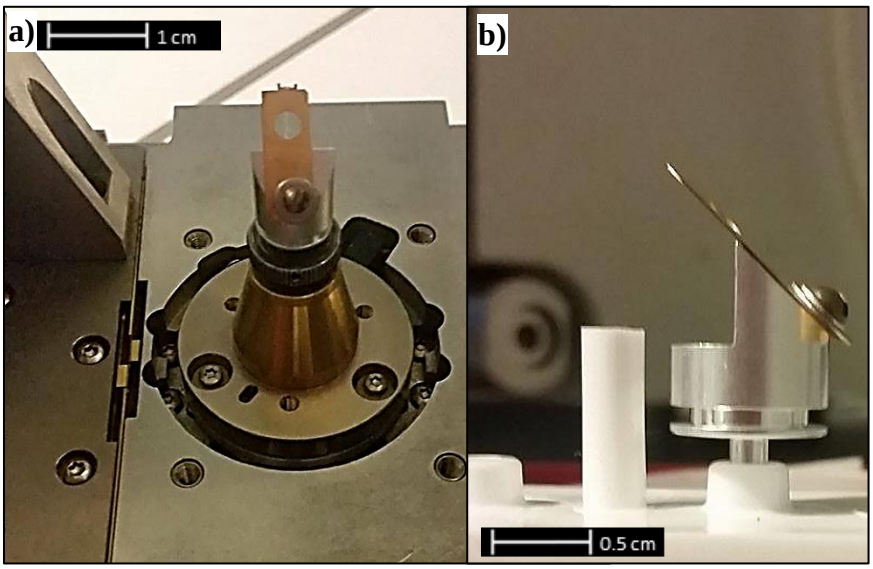

Figure 9. Steel TKD Holder Prototype by J. Orsborn

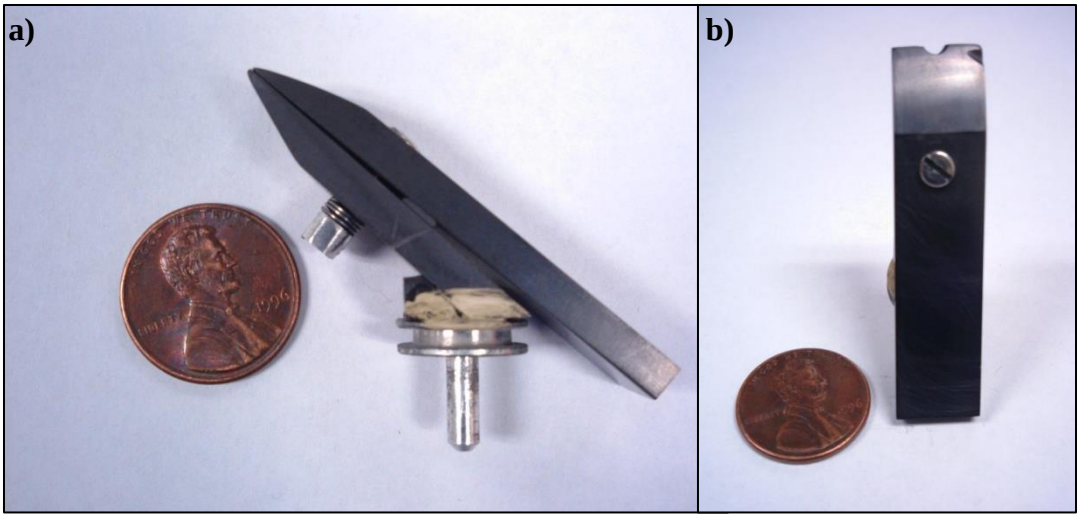

Figure 10. Graphite TKD Holder Prototype by S. R. Arango

3.2 Sample Preparation

A cross section of the friction stir weld was cut and mounted in 1.5” bakelite, and ground with sandpapers up to 1200 grit with at least 30 seconds of ultrasonication in an ethanol bath. It was further polished using diamond suspension and colloidal silica to 0.5 μm. The mounted sample was then etched with 2% Nital solution for 5 s in order to obtain light etching of the steel for visibility of the weld interface. A macrograph of the

weld and the interface area at which the TKD thin foil is taken from is shown in Figure 11 below. The samples were then taken to a Helios Focused Ion Beam (FIB) for thin foil extraction at the interface

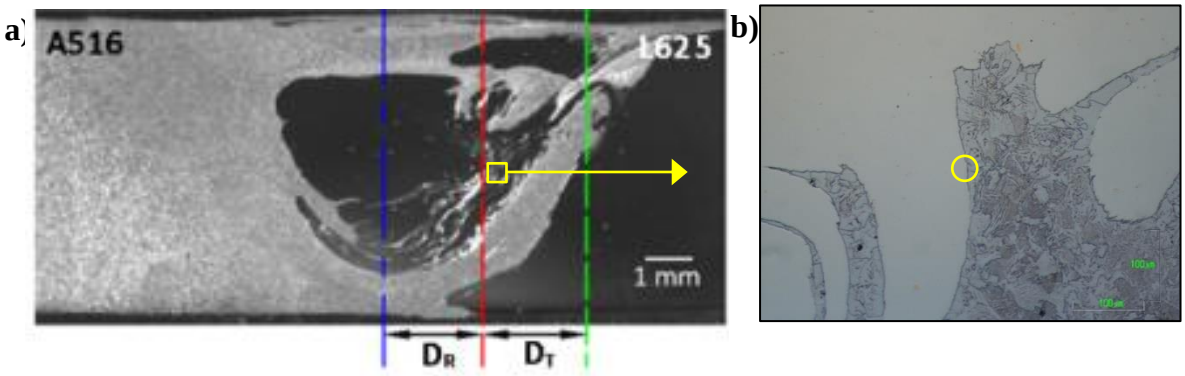

Figure 11. Macrograph of FSW and Interface

The created foil was thinned to approximately 30x5x0.2 µm, plasma-cleaned, and further polished by a Fischione Nano-mill Ion Beam to eliminate affected layers from the extraction and thinning process. Figure 12 shows the thin foil sample at the Nickel-Steel weld interface mounted to an Omniprobe copper grid. After several scans and analyses with the same foil, further cleaning and polishing is required to eliminate oxide buildup.

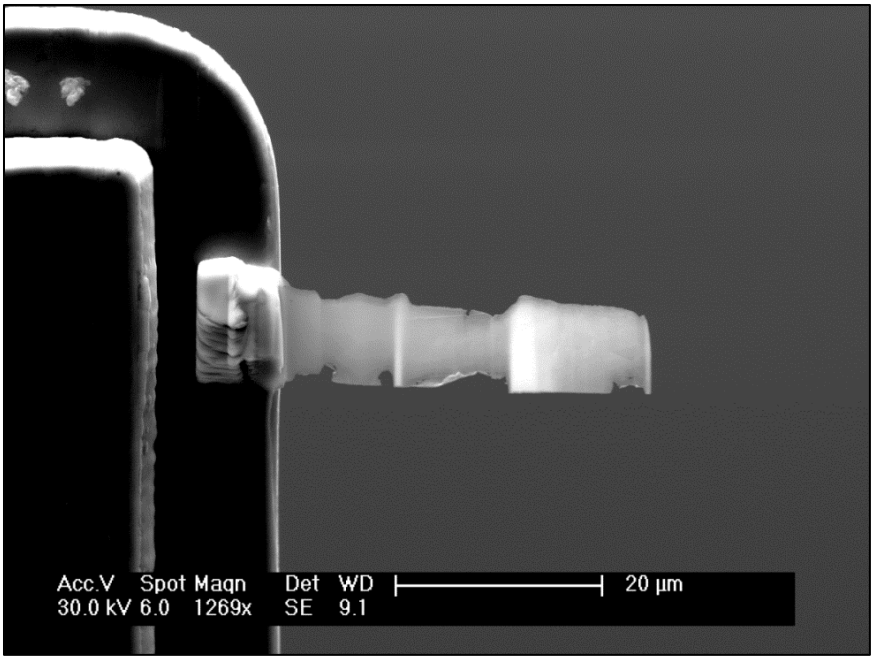

Figure 12. TKD Thin Foil at Nickel-Steel Weld Interface

3.4 Characterization and Analysis

Preliminary optical and SEM imaging characterization was conducted on the bulk cross section in order to locate the optimal location for foil extraction. SEM imaging, TKD and X-EDS analyses were run in CEMAS's XL-30 ESEM. Calibration at working distances of 4-8 mm was conducted using silicon single crystal samples. The steel and aluminum TKD holders were used for TKD analysis, and the aluminum and graphite holders were used for simultaneous TKD and X-EDS mapping. Imaging and analyses were all conducted with electron beam accelerating voltage of 30 kV, spot size of 6, and aperture at 100 µm. TKD analyses were conducted at working distance of 4 mm and simultaneous TKD and X-EDS was run at 5 mm working distance to prevent shadowing from the SEM pole piece. Mapping was conducted with step sizes of 10 nm unless otherwise specified.

Chapter 4: Results and Discussion

4.1 Stir Zone Microstructure

Widmanstätten and grain boundary ferrite as well as pearlite grains were identified in the A516 steel stir zone. The stir zone of Ni-625 contained an austenite matrix and no visible precipitates by optical microscopy within the stir zone adjacent to the joint interface.

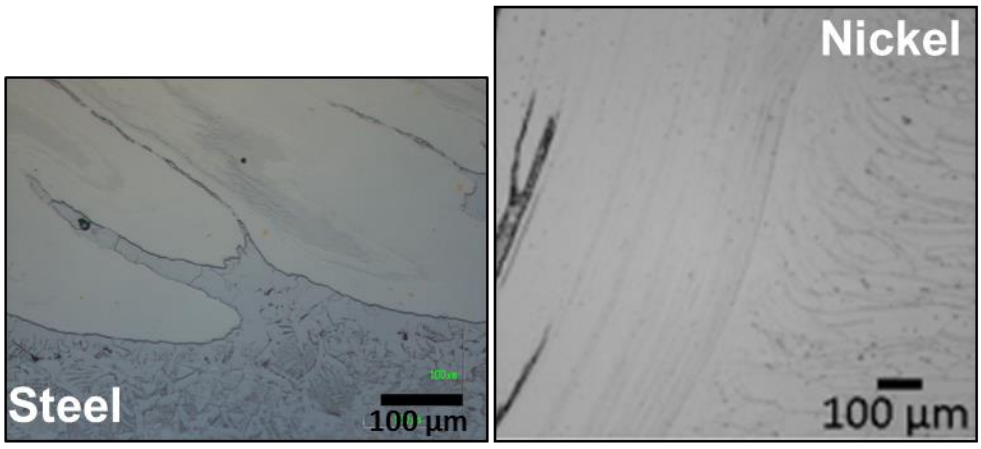

Figure 13. Microstructure of Stir Zones

This corresponds to microstructures of A516 and Ni-625 FSW studies done by J. Rodriguez [17] and K. H. Song [6].

4.2 TKD Analysis

TKD analysis was run on the thin foil created at the weld interface. The aluminum and steel holders were used because the chemical composition of the holders did not affect the data. TKD maps of the nickel-steel interface between the welds are scanned with a step size of 6 nm, shown below in Figure 14. The images depict the TKD

crystallographic orientation of the weld intersection regions, and the two images below show only BCC Ferrite grains of the Steel and only FCC Austenite Nickel grains.

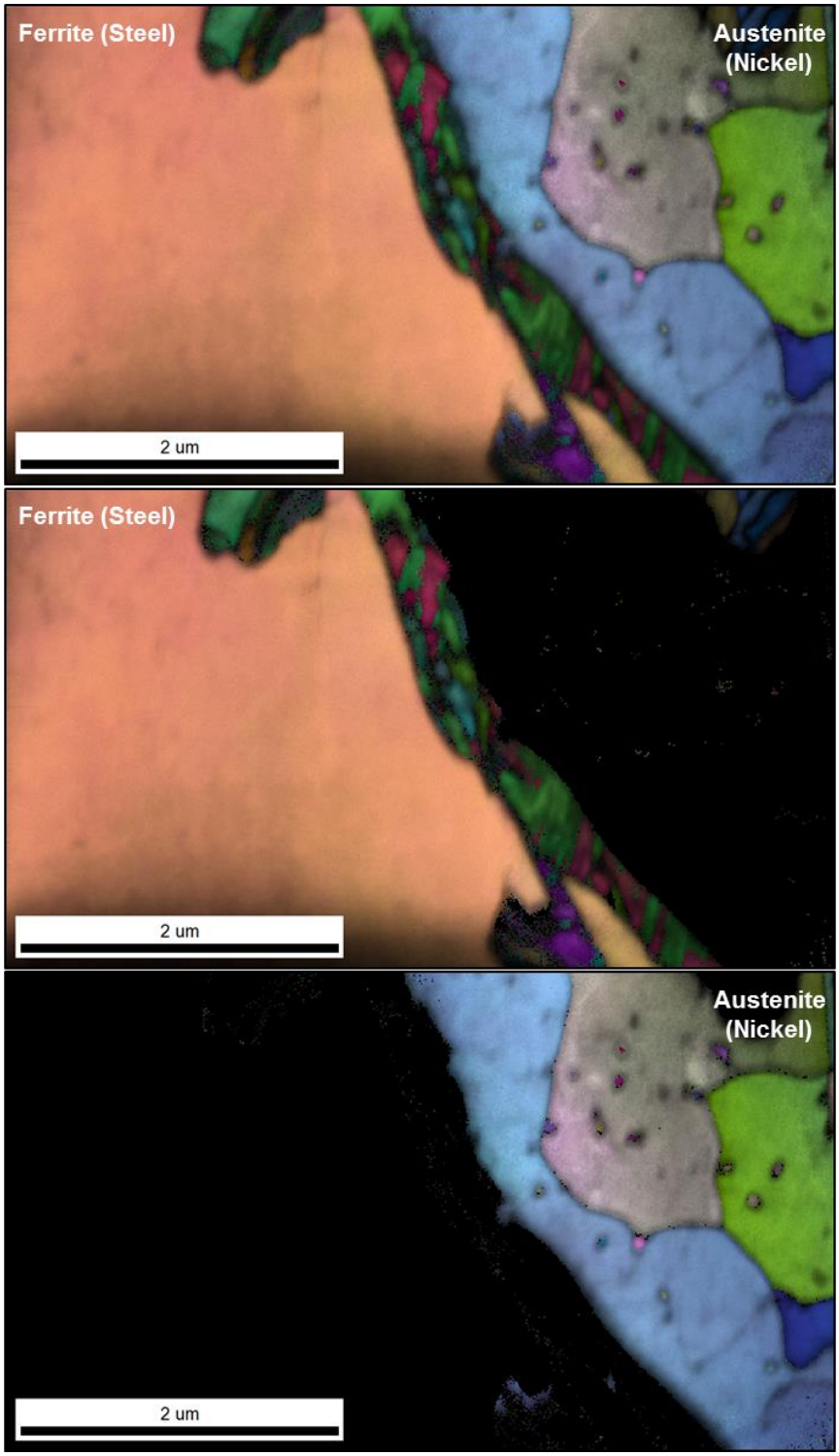

Figure 14. TKD IQ+IPF Map of Interface

When identifying phases, generally, better image quality of diffraction patterns will result in higher Confidence Indexes (CI), or the confidence in the identification of the TKP diffraction pattern. However, there can be error in the software when identifying phases, especially when high strain is encountered, or at grain boundaries where signals and patterns of adjacent grains may overlap. The grains on the right of the interface are in the Ni-based alloy 625 stir zone, and are relatively small, approximately 1 μm wide. Some precipitates can be observed in grains and grain boundaries. On the ferrite side, there are much larger grains in the stir zone region but fine grains along the boundary of the interface.

In the Ni-based alloy stir zone, the grains exhibit FCC austenite structured matrix and precipitates about 50 nm at grains and grain boundaries. From previous work with FSW of these alloys, these precipitates are most likely Niobium Carbides (NbC) with other MC system carbides: MC, M6C, M23C6 [17]. The mapping software cannot differentiate between the FCC austenite matrix and the precipitates correctly, exemplified in Figure 15, though the TKP of the two differ (Figure 16).

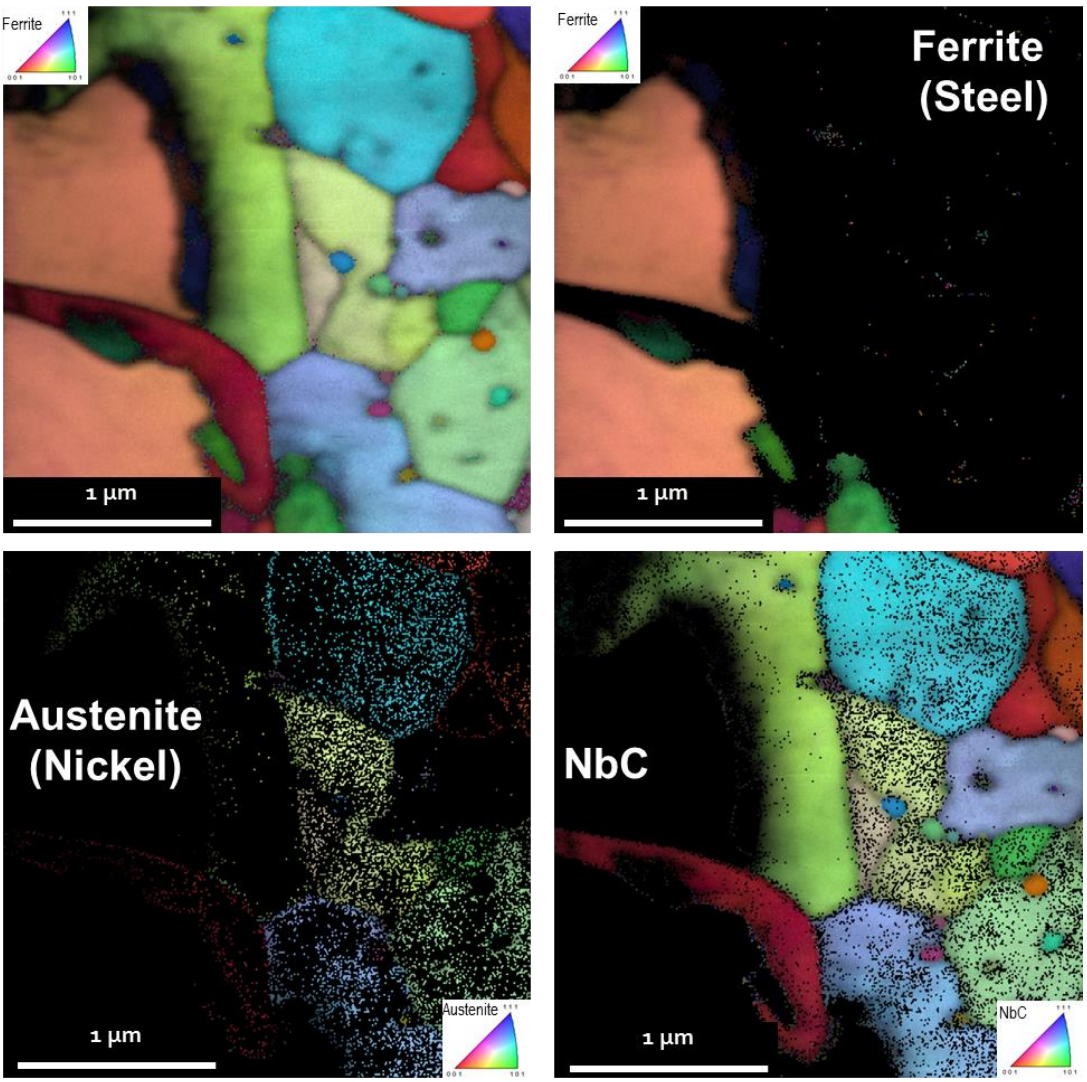

Figure 15. Incorrectly Indexed Crystallographic Maps

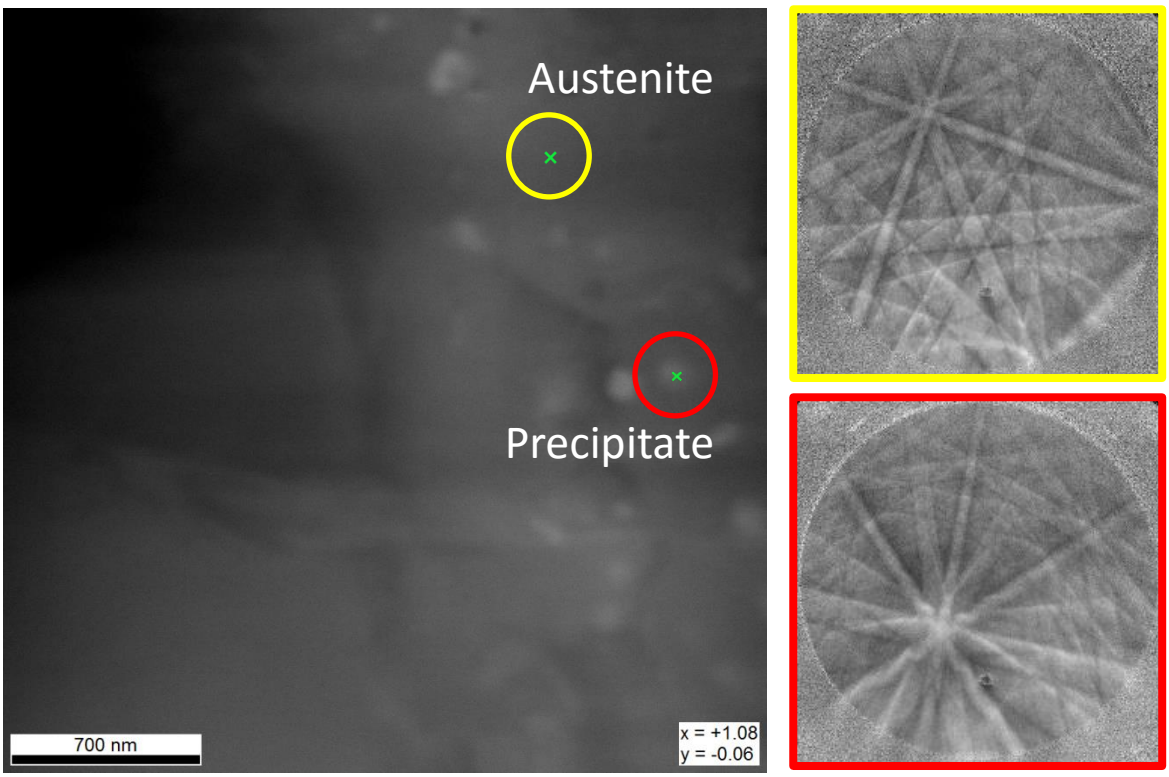

Figure 16. TKP of Austenite and Precipitate

Above, the austenite matrix should comprise most of the right side of the TKD map and the smaller precipitates should present as a separate phase, however the Ni-based alloys are identified as both. Using X-EDS to filter crystal structures by chemical composition, these precipitates can be more accurately identified – further explained in Chapter 4.3 Simultaneous TKD and X-EDS Analysis.

The Steel A516 stir zone of the interface, contains no visible precipitates and fine, grains along the interface identified as BCC ferrite with lower IQ values, as diffraction patterns here are much less distinct, as seen in Figure 17. This may indicate high strain along this region, possibly due to shearing in the FSW process, or the presence of martensite, a metastable, Body Centered Tetragonal (BCT) crystal structure similar to that of strained BCC ferrite.

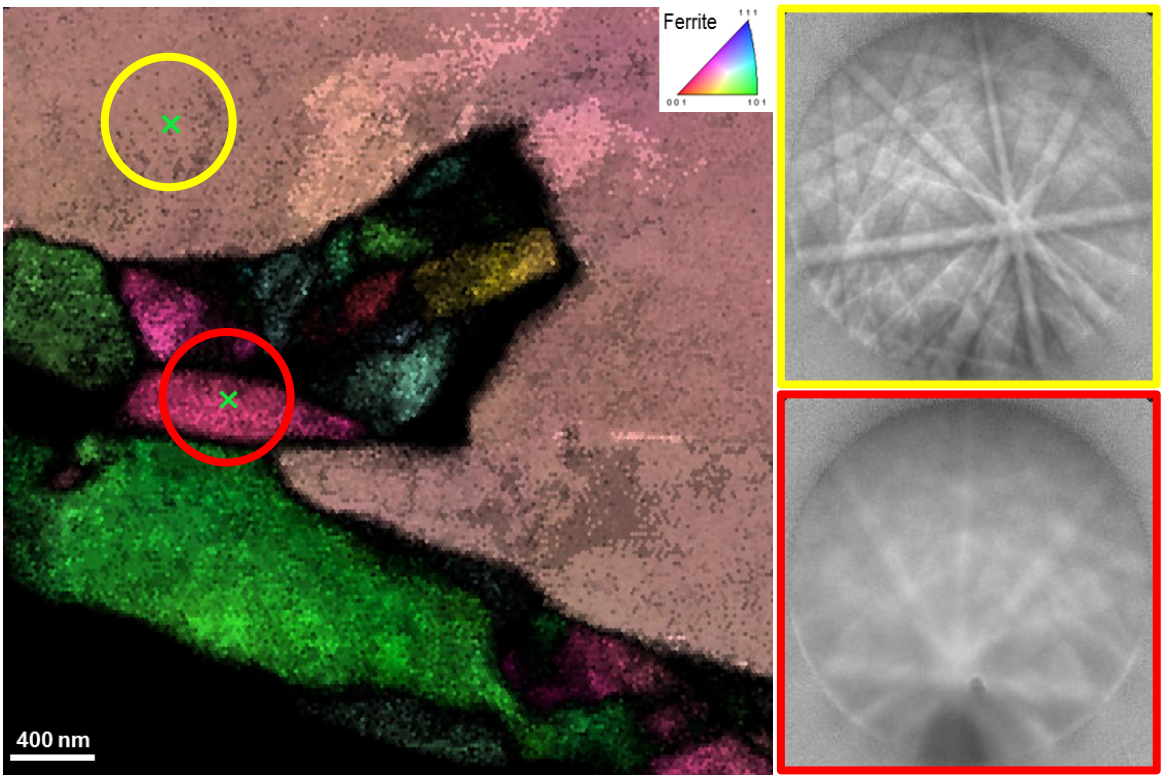

Figure 17. TKP Patterns of Ferrite

TKD provides crystal structure and orientation of the thin foil specimen, and the austenite and ferrite crystal matrix may have a range of elemental composition. TKD alone does not absolutely distinguish any intermixing region at this weld interface, and discerning the compositional gradient that may exist at this region requires other methods.

4.3 Simultaneous TKD and X-EDS Analysis

X-EDS provides chemical composition data from the thin foils within the sample in the SEM. Current software allows for simultaneous scanning with TKD and X-EDS. The elements of interest were iron, nickel, chromium, molybdenum, and molybdenum, and 10 nm step sizes were used for all mapping. Figure 18 below depicts maps collected during TKD and X-EDS scans. The first image is a crystallographic map, the second is a phase map created using indexed patterns from the first map, and the last illustrates X-EDS chemical composition at the same area.

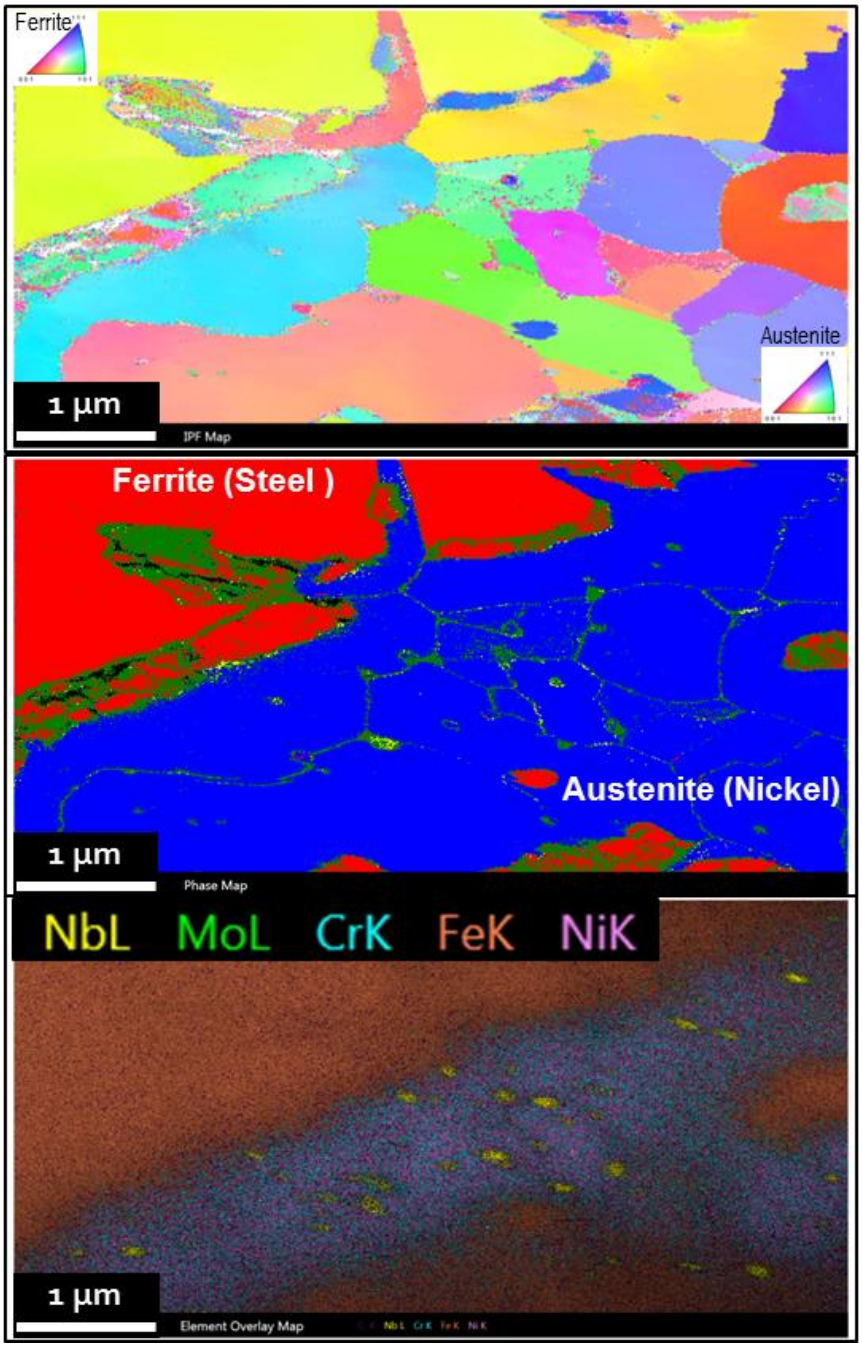

Figure 18. Maps of Simultaneous TKD and X-EDS

The X-EDS map shows regions of iron and a solution of nickel and chromium with small particles of niobium. The niobium constituents are at in the austenite regions of the TKD maps, and are the approximate size of the precipitates seen in the crystallography maps. Furthermore, X-EDS scans in Figure 19 show that the precipitates have little or no iron,

chromium, or nickel. Molybdenum was not included in this scan, but a second scan seen in Figure 20 was run on the same area and it was found in nearly all precipitates where niobium was present.

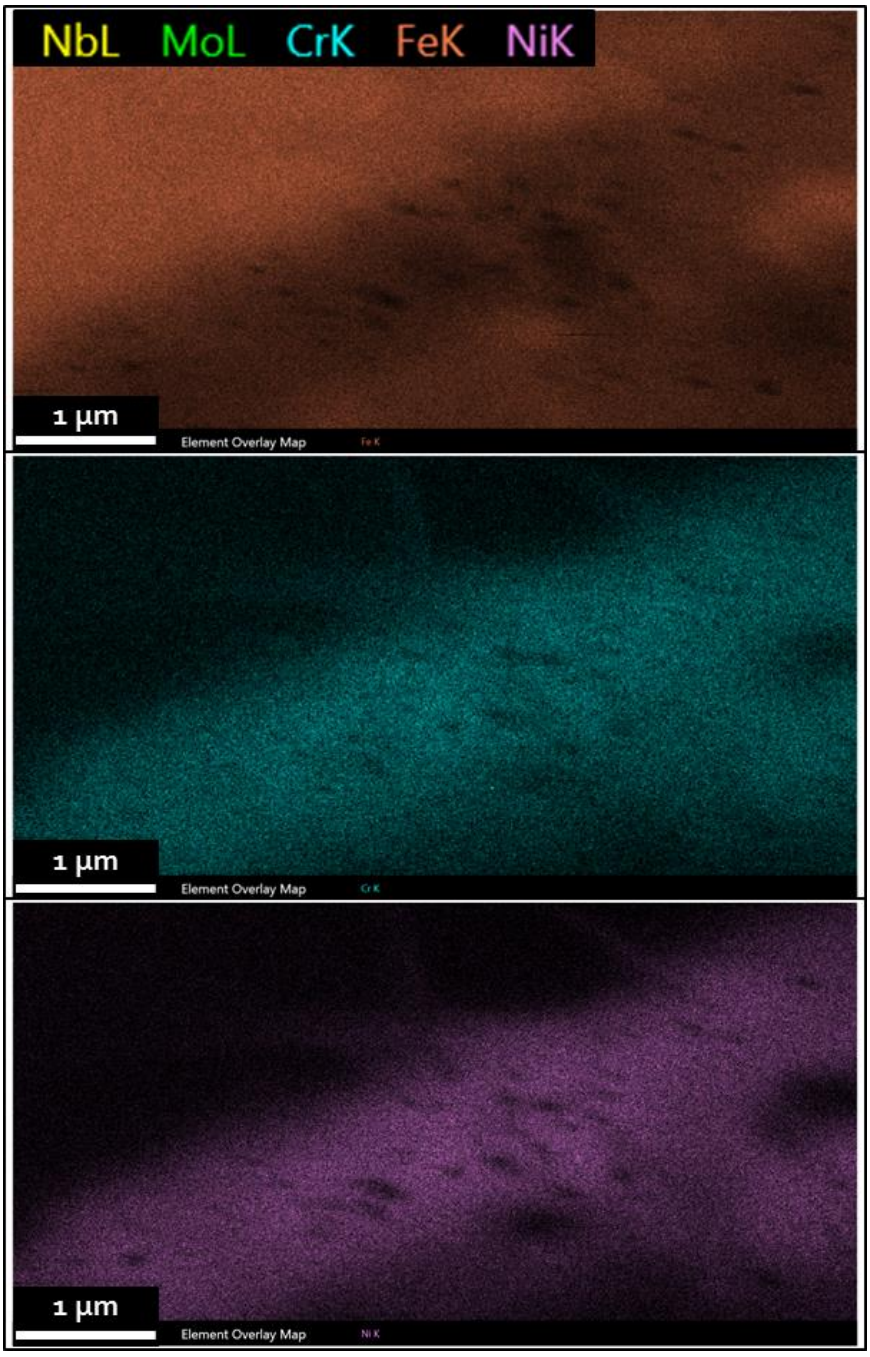

Figure 19. X-EDS Mapping of Fe, Cr, Ni

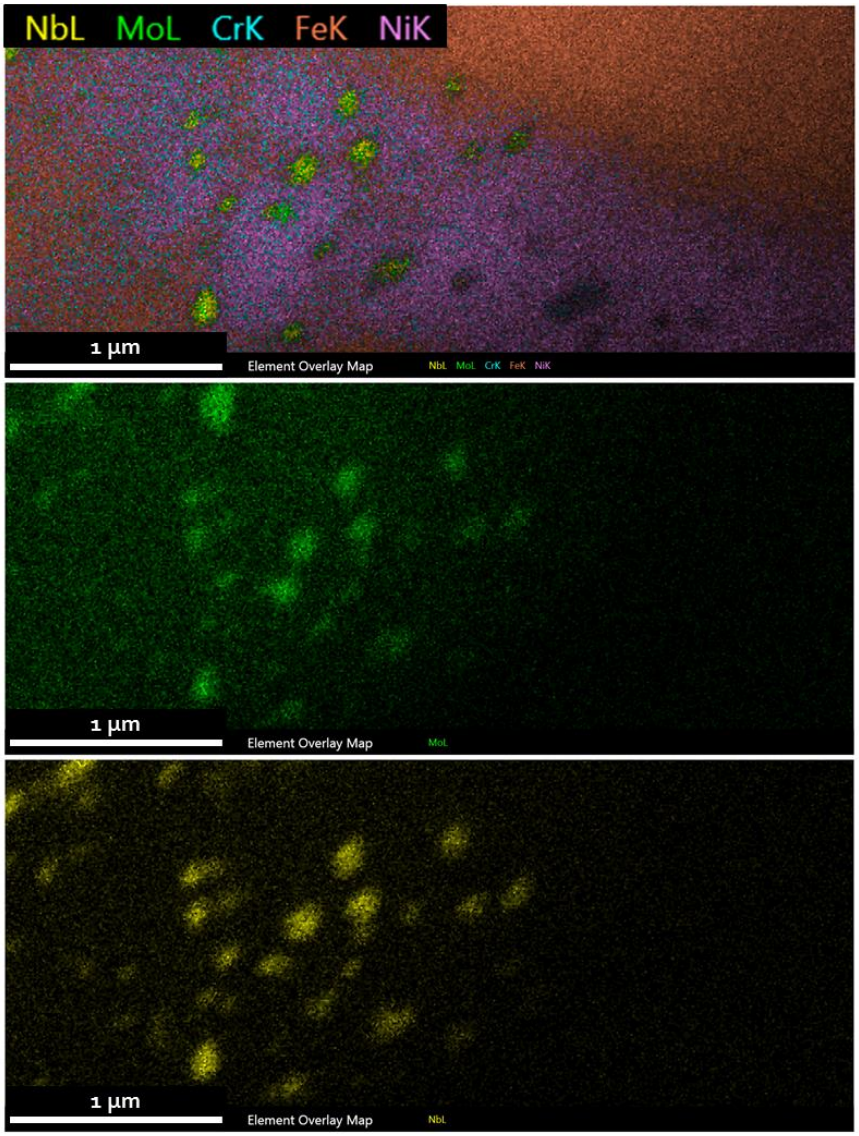

Figure 20. Second Scan of X-EDS Mapping of Mo, Nb

However, the phase diagram, Figure 24 of Appendix A, and other studies of Ni-based Alloy 625 show no mention of a precipitate with only niobium and molybdenum (

Table 2 in Appendix A). X-EDS identification relies on the characterization of X-ray energy peaks on a collected spectrum, and characteristic niobium and molybdenum x-rays are similar enough that there may be errors in distinguishing between niobium and molybdenum. A sample spectrum for a precipitate is shown below in Figure 21, and the measured energy peaks are nearly indistinguishable. More work must be done to understand the presence of molybdenum in these precipitates conclusively.

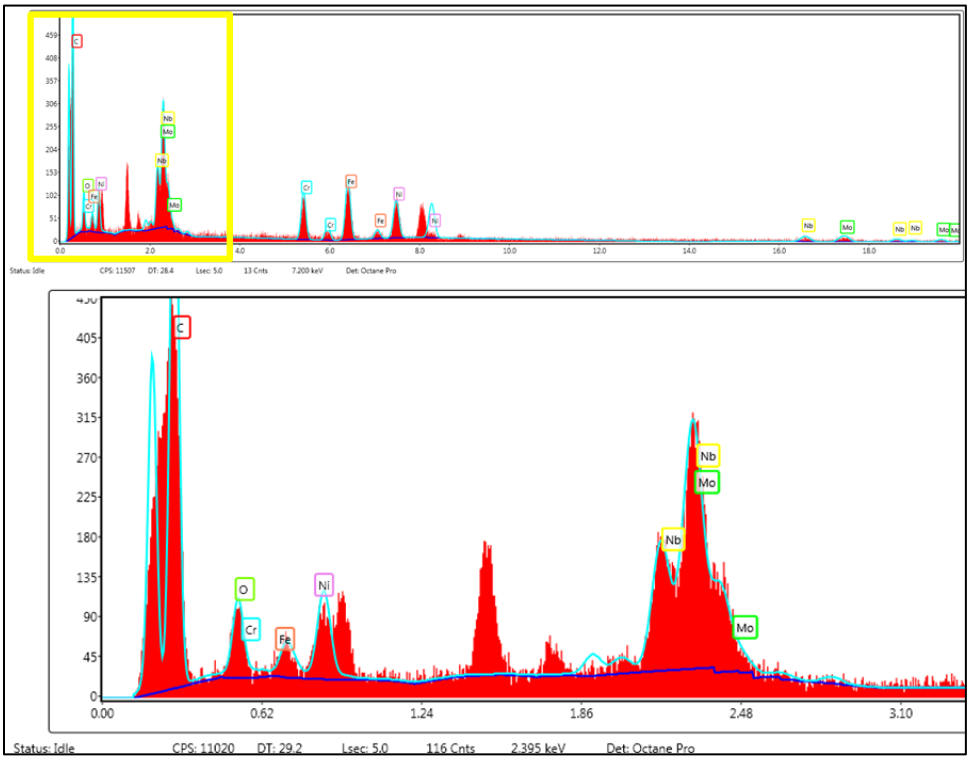

Figure 21. X-EDS Energy Spectrum for Precipitate

Using chemical filtering and crystallographic analysis, further detailed in 4.4 Chemical-Assisted Indexing, these precipitates may be correctly categorized.

4.4 Chemical-Assisted Indexing

Using chemical-assisted indexing, the TKD orientation mapping can be set to yield more accurate identification of crystal structures at the sample interface region. Structures in the interface can produce TKPs of similar structure or lattice parameter, and

this function of the data analysis software can eliminate or relegate the likelihood of incorrect identification of crystal structures by filtering choices based on X-EDS composition data at a given map location. In the example with Figure 15, the composition of the nickel matrix will reduce the probability of its identification of niobium carbide, and the niobium carbides should be correctly assigned the NbC crystal structure. Using this function on the software, the reprocessed map at the bottom of Figure 22 is created. The original crystal structure and chemical composition maps are shown at the top. There is greater success in correctly identifying precipitates in the austenite nickel matrix; however the interface between ferrite and austenite is less defined.

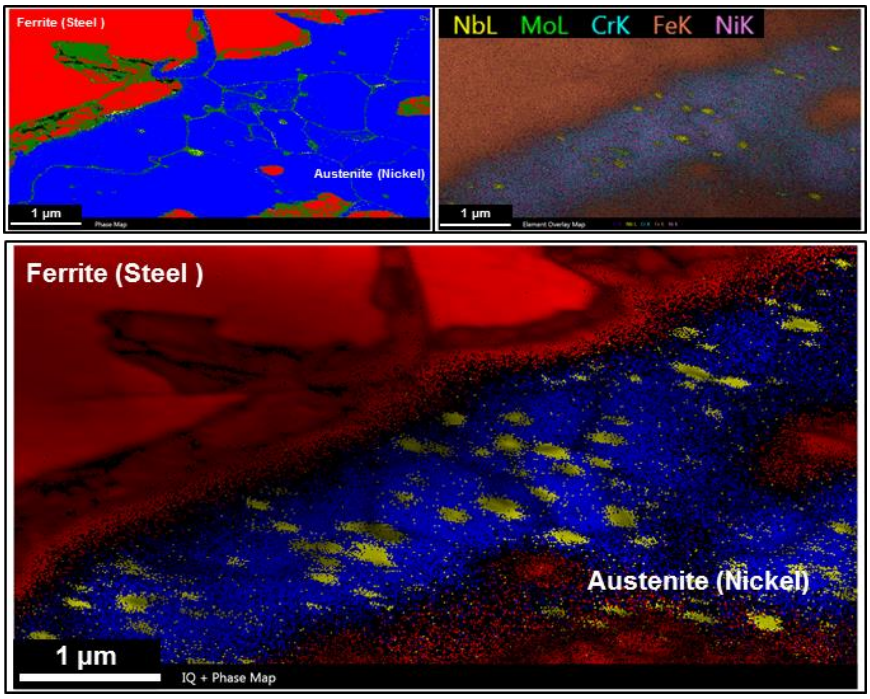

Figure 22. Chemical Assisted Scan

No successful or conclusive maps including Cr6C or Cr23C6 phases were obtained.

Chapter 5: Conclusions and Future Work

5.1 Conclusions

Friction stir welds between Ni-based alloy 625 and low-carbon steel ASTM A516 were analyzed using Transmission Kikuchi Diffraction and Energy Dispersive X-ray Spectroscopy for characterization. The Steel A516 stir zone at the interface contained BCC ferrite morphology with fine grains on the order of ~300 nm at the interface. These grains exhibited poor diffraction patterns, which may be indicative of high strain from the joining process or resultant phase transformations. The stir zone of the Ni-based alloy consists of an FCC austenite nickel matrix with both intra- and intergranular NbC carbides approximately ~50 nm across. The compositional gradient region at the interface is measured to be approximately 1-2 μm wide in the FCC Austenitic crystallographic region.

5.2 Impact

Characterization of FSWs between Ni-based Alloy 625 and low-carbon Steel A516 at spatial resolutions in nanometers provides more through detailing of the microstructures and features of these joints. This in turn can be used to extrapolate the morphology of these regions as well as any physical properties that result from joining these materials in this fashion, especially in similar material studies to where weldability

or material issues are inexplicable. Furthermore, the work done can be utilized in future studies and applications of similar welds on these types of alloys.

Although there are no heavily used applications of friction stir welding between Ni-based alloys and steels, this study furthers the work done to qualify the process between these two materials for implementation in industry. Currently used in the aeronautical field on aluminum alloys, these welds could be favorable for similar large, long welds on Ni-alloyed and steel manufacturing pipes and pressure vessels.

The work done to develop TKD at Ohio State yields even greater implications in the university materials characterization community. With rapid but detailed analyses at spatial resolutions up to 10 nm, more data can be obtained from regions with fine features that formerly required analysis with the Transmission Electron Microscope (TEM) – requiring high levels of training and skill to run on a smaller area of analysis than TKD. Moreover, the additional expense of conducting TEM analyses may deter higher resolution data collection on studies, where TKD on the SEM will necessitate less training and greater scan speeds at similar resolutions at the TEM. This process is not limited to metallic or materials investigation, as TKD microscopy may be employed in a variety of research fields.

5.3 Future Work

Further analysis will be done on the identification of the fine grains within the steel interface region. Because carbon compositions cannot be obtained using X-EDS and BCT Martensite is not discernable from BCC Ferrite by TKD methods, indenting methods will be used to detect the presence of the hard and brittle metastable microstructure. Common indentation techniques such as macro- and microhardness,

analyzes an area significantly larger than the size of the grains in the FSW of Ni-based alloy and steel, as indentations measure micrometers across. Nanoindentation is a technique that can process hardness indentation information at the nanometer scale and extrapolate a range of physical and material properties, unlike the previously mentioned indentation methods.

Additionally, the thickness of the foil creates noise and discrepancies between the TKD and X-EDS analyses. Illustrated by Figure 23, the foil is about 0.5 µm, and the analyses come from different layers of the foil thickness. Diffraction patterns from TKD are generated from the bottom 10-20 nm of the foil, while X-EDS characteristic x-rays are generated by the entire thickness of the foil.

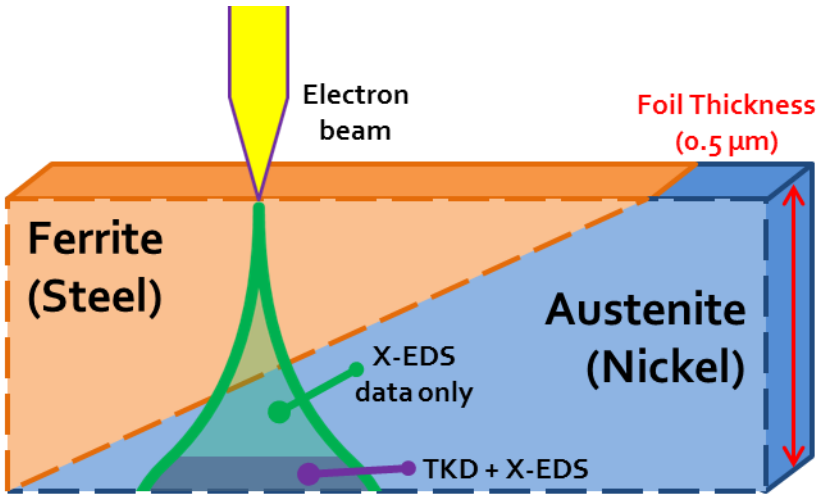

Figure 23. Discrepancies from Foil Thickness

In the figure above, X-EDS will detect Ferrite and Austenite presence, while TKD recognizes only Austenite at this area. Determining the location of the gradient compositional region with respect to the crystallographic Ferrite-Austenite interface may be done by running scans from both sides of the foil with plasma cleaning between steps.

Future work will be conducted on foil samples originating at different areas of the same FSW cross section, particularly near the shoulder of the FSW tool during welding. The metallurgical phenomena resulting from the stirring process beneath the shoulder differ from the region in the center of the stir weld, and have been shown to produce separate microstructures and material properties [17]. Other samples within the same weld will be analyzed for possible variation in microstructure and morphology.

These same analyses will be made upon interfaces of various dissimilar metal welds. Aluminum-to-steel dissimilar welds are used in industry and have the potential for implementation within many other manufacturing fields. However, interest for characterizing such welds exists in identifying the presence of detrimental intermetallic compounds forming between Aluminum and Steel. With quick joining processes like SS impact or explosion welding, these intermetallics may be nanometers small, and TKD/X-EDS analysis will be highly applicable for swift, high resolution characterization and analysis.

Appendix A

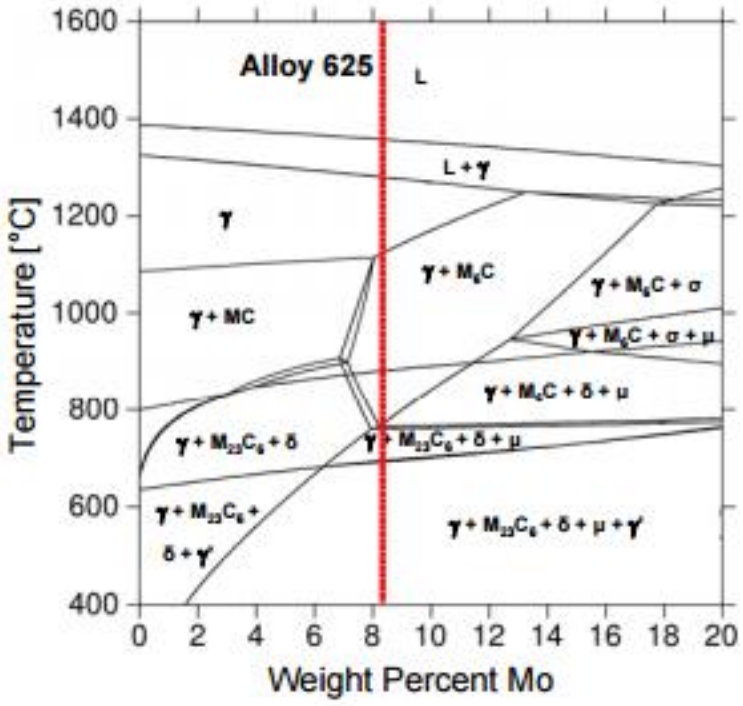

Figure 24. Phase Diagram of Ni-Based Alloy 625 [19]

Table 2
Phases and Precipitates Observed in Ni-Based Alloy 625 and ASTM A516 [20] [21]

Phase	Structure	Lattice Parameter (nm)	Composition
γ	Cubic (FCC)	0.357-0.3607	Solid Solution
MC	Cubic	0.43-0.4449	(Nb) C
		0.43-0.4427	(Nb, Ti) C
M6C	Cubic	1.13	(Cr, Mo, Ni)6C
M23C6	Cubic	1.08	Cr23C6
Laves	Hexagonal	0.47	(Cr, Ni)2(Nb, Mo)
γ"	Ordered Tetragonal	0.36	Ni3(Nb, Ti, Al)
δ	Orthogonal	0.51	Ni3Nb
(Cr, Nb)2N	tetragonal	0.3	(Cr, Nb)2N

Table 3
X-EDS Energy Peaks for Elements of Interest [22]

Element	Symbol	Kα	Lα
Iron	Fe	6.398	0.705
Nickel	Ni	7.471	0.851
Chromium	Cr	5.411	0.573
Molybdenum	Mo	17.441	2.293
Niobium	Nb	16.581	2.166
Aluminum (TKD Holder)	Al	--	0.277
Carbon (TKD Holder)	C	--	1.486

References

[1] S. Wang, J. Ding, H. Ming, Z. Zhang and J. Wang, "Characterization of low alloy ferritic steel -- Ni base alloy dissimilar metal weld interface by SPM techniques, SEM/EDS, TEM/EDS and SVET," *Materials Characterization,* vol. 100, no. 1, pp. 50-60, 2015.

[2] B. T. Alexandrov, J. C. Lippold, J. W. Sowards, A. T. Hope and D. R. Saltzmann, "Fusion boundary microstructure evolution associated with embrittlement of Ni–base alloy overlays applied to carbon steel," *Weld World,* vol. 57, no. 1, pp. 39-53, 2013.

[3] Z. S. Pereira and E. Z. da Silva, "Cold Welding ofGold and Silver Nanowires:AMolecular Dynamics Study," *Journal of Physical Chemistry,* vol. 115, no. 1, pp. 22870-22876, 2011.

[4] T. J. Ma, M. Yan, X. Yang, W. Li and Y. J. Chao, "Microstructure evolution in a single crystal nickel-based superalloy joint by linear friction welding," *Materials and Design,* vol. 85, no. 1, pp. 613-617, 2015.

[5] T. J. Ma, X. Chen, W. Y. Li, X. W. Yang and S. Q. Yang, "Microstructure and mechanical property of linear friction welded nickel-based superalloy joint," *Materials and Design,* vol. 89, no. 1, pp. 85-93, 2016.

[6] K. H. Song and K. Nakata, "Mechanical Properties of Friction-Stir-Welded Inconel 625 Alloy," *Materials Transactions,* vol. 50, no. 10, pp. 2498 - 2501, 2009.

[7] K. H. Song and K. Nakata, "Effect of precitation on post-heat-treated Inconel 625 alloy after mfriction stir welding," *Materials and Design,* vol. 31, no. 1, pp. 2942-2947, 2010.

[8] T. J. Lienert, W. G. Stellwag, B. B. Grimmett and R. R. Warke, "Friction Stir Welding Studies on Mild Steel," *Welding Journal,* vol. January, pp. 1s-9s, 2003.

[9] Y. C. Lim, S. Sanderson, M. Mahoney, X. Yua, D. Qiao, W. Zhang and F. Feng, "Characterization of Multilayered Multipass Friction Stir Weld on ASTM A572 G50 Steel," *Welding Journal,* vol. 93, pp. 1s-8s, 2014.

[10] J. Rodriguez and A. J. Ramirez, "Microstructural characterisation of friction stir welding joints of mild steel to Ni-based alloy 625," *Materials Characterization,* vol. 110, no. 1, pp. 126-135, 2015.

[11] TWI Ltd., "Joining Technologies," TWI, 2016. [Online]. Available: http://www.twi-global.com/capabilities/joining-technologies/. [Accessed 5 April 2016].

[12] S. W. Kallee, E. D. Nicholas and W. M. Thomas, "Industrialisation of friction stir welding for aerospace structures," in *Structures and Technologies - Challenges for Future Launchers,* Strasbourg France, 2001.

[13] J. Rodriguez and A. J. Ramirez, "Friction stir welding of mild steel to alloy 625," *Science and Technology of Welding and Joining,* vol. 19, no. 4, pp. 343-349, 2014.

[14] Z.-W. LIU, A. J.-J. HU, C.-C. LIN, C.-F. JIANG and Y. ZENG, "Application of Transmission Electron Backscattered Diffraction in Nanomaterials Research," *Journal of Inorganic Materials,* vol. 30, no. 8, pp. 833-837, 2015.

[15] A. J. Schwarts, M. Kumar, B. L. Adams and D. P. Field, Electron Backscatter Diffraction in Materials Science, Second ed., New York: Springer Science+Business Media, LLC, 2000.

[16] Oxford Instruments, "EBSD Explained," 2015. [Online]. Available: oxford-instruments.com/EBSD. [Accessed 6 April 2016].

[17] J. R. Fernandez, *Microstructural characterization of ASTM A516 - Ni based alloy 625 friction stir welded joints,* (Doctoral dissertation). Universidade Estadual de Campinas, 2013.

[18] S. Langner, "Microanalysis News July 2014," July 2014. [Online]. Available: http://my.bruker.com/acton/media/2655/bruker-microanalysis-news---july-2014. [Accessed 22 March 2016].

[19] J. C. Lippold, J. W. Sowards, G. M. Murray, B. T. Alexandrov and A. J. Ramirez, "Weld Solidification Cracking in Solid-Solution Strengthened Ni-Base Filler Metals," in *Hot Cracking Phenomena in Welds II*, Springer, Ed., Berlin, Springer Berlin Heidelberg, 2008, pp. 147-170.

[20] JEOL USA, Inc., "JEOL USA Electron Optics Documents and Downloads," 2016. [Online]. Available: http://www.jeolusa.com/DesktopModules/Bring2mind/DMX/Download.aspx?EntryId=386&Command=Core_Download&language=en-US&PortalId=2&TabId=320. [Accessed 4 April 2016].

[21] S. Floreen, G. E. Fuchs and W. J. Yang, "The Metallurgy of Alloy 625," TMS, Schenectady, 1994.

[22] C. C. Silva, H. C. de Miranda, M. F. Motta, J. P. Farias, C. R. M. Afonso and A. J. Ramirez, "New insight on the solidification path of an alloy 625," *J Mater. Res. Technol.*, vol. 2, no. 3, pp. 228-237, 2013.